Functionalisation and stabilisation of polymeric arsenical nanoparticles prepared by sequential reductive and radical cross-linking

*Joji Tanaka[‡f], Alexander Evans[‡], Pratik Gurnani[†], Andrew Kerr, Paul Wilson**

University of Warwick, Department of Chemistry, Coventry, CV4 7AL, UK

ABSTRACT

The chemical reactivity of arsenic is diverse and distinctive depending upon its interchangeable oxidation states. Alkyl and aryl arsines (As(I)) exist as oligomers, composed of labile and redox responsive As-As bonds which have been exploited to form reactive and responsive materials. Here, the lability and reactivity of As(I)-functional polymeric nanoparticles, derived from thermoresponsive polymers P(PEGA$_{20}$-*b*-[NIPAm$_{80-n}$-*co*-AsAm$_n$]) (**P1**, n = 4; **P2**, n = 11; **P3**, n = 15; **P4**, n = 18), is elaborated by *in-situ* reaction with functional acetylenes, resulting in the formation of vinylene-arsine cross-linked polymeric arsenical nanoparticles (**NP$_{V\text{-}As}$**). Spherical particles with sizes < 35 nm have been prepared, which are adventitious for potential drug-delivery (e.g. tumour accumulation) applications. Functional acetylenes enable the introduction of reactive amine, acid and alcohol functional groups into the particles, while the use of propargyl-*O*-rhodamine ester results in the formation of fluorescent nanoparticles. The vinylene-arsine cross-linking confers increased stability of the polymeric arsenical nanoparticles in model biological redox conditions (GSH, H_2O_2, 5 mM) compared to those reported previously, with nanoparticle structures retained over 7 days. The parent polymeric arsenicals and the resulting

nanoparticles were all shown to exhibit limited cytotoxicity *in vitro* and cell uptake was confirmed by incubating fluorescent-labelled nanoparticles with PC3 cells. Furthermore, fluorescent confocal microscopy using the PC3 cell-line, confirmed that the nanoparticles were internalised by the cells with evidence of mitochondrial co-localisation, which supports a mitochondria-targeting of arsenic hypothesized based on work involving organoarsenical chemotherapeutics. Thus, this work demonstrates a novel strategy for the preparation of polymeric arsenical nanoparticles, with broad functional group tolerance, and expanded our emerging understanding of the *in-vitro* behaviour of this family of nanomaterials.

INTRODUCTION

The use of arsenic trioxide (Trisenox, As_2O_3) for effective treatment for acute promyelocytic leukaemia (APL) has revitalised the therapeutic potential of (in)organic arsenicals.[1] Organic arsenicals 4-(*N*-(*S*-glutathionylacetyl)amino) phenylarsonous acid (GSAO),[2] 4-(*N*-(*S*-penicillaminylacetyl)amino) phenylarsonous acid (PENAO)[3] and S-dimethylarsino-glutathione (ZIO-101; Darinasparin)[4] have gained much attention for use as mitochondrial targeting chemotherapeutic drugs, demonstrating higher potency and reduced cytotoxicity compared to inorganic counterparts. The activity of these trivalent organic arsenical (As(III)) drugs is attributed to their high affinity for proximal dithiols,[5, 6] which are abundant in redox active proteins responsible for a number of crucial roles within the intracellular space, such as post-translational protein folding and redox homeostasis.[7-9] For example, it has been postulated that GSAO and PENAO disrupt the mitochondrial membrane potential by cross-linking Cys^{57} and Cys^{257} of mitochondrial adenine nucleotide translocase (ANT), leading to opening of the mitochondrial permeability transition pore (MPTP).[10]

The clinical renaissance of (in)organic arsenicals is beginning to manifest broader acceptance of the use of organic arsenicals in the field of polymer and (bio)materials science.[11] Recently, Stenzel and co-

workers have synthesised a PENAO-derived methacrylamide monomer and copolymerized it into the hydrophilic, corona-forming block of amphiphilic block copolymers to fabricate PENAO-functional polymeric nanoparticles.[12] The presence of pendent thiol-philic As(III) groups was chemically confirmed by mono and dithiol substitution reactions and incorporation of PENAO into the corona of polymer nanoparticles was shown to improve the activity and cell uptake relative to PENAO alone. Moreover, in agreement with the proposed activity of PENAO, the As(III)-functional nanoparticles exhibited mitochondrial colocalisation alluding to the potential for active targeting with organelle specificity. Polymerisation-induced self-assembly (PISA) has also been employed to demonstrate the role and effect of the stabilizing (hydrophilic) PENAO-containing block on the reactivity and cytotoxicity of PENAO-functional nanoparticles, whereby shorter, more-condensed stabilizing blocks exhibited up to 5-fold increase in toxicity.[13]

The (bio)chemical reactivity and biological activity of arsenic is richly diverse and can be distinctive, depending upon its oxidation state, of which As(V), As(III) and As(I) can be considered to be biologically relevant. With this in mind we have adopted the long-term aim of developing polymeric arsenicals as a platform for functional (bio)materials wherein both the chemical reactivity and biological activity are accessible functions of the materials, typically in response to biological stimulus. Initially, α-As(V)-functional (co)polymers were synthesized by aqueous single electron transfer living radical polymerisation (Aq-SET-LRP). The As(V) chain-end was readily reduced to As(III) in the presence of glutathione and the resulting polymers were shown to undergo highly efficient and reversible conjugation *via* re-bridging of reduced disulfides.[14] The versatility, degree and controlled incorporation of As-functionality present in polymeric arsenicals has been expanded using simple organic arsenical acrylamide monomers (AsAm) derived from commercially available *p*-arsanilic acid. Reversible addition fragmentation chain-transfer (RAFT) polymerisation has been employed to prepare polymeric arsenical scaffolds for post-polymerization modification of the pendent As(V) groups *via* sequential

reduction (to As(III)) and thiol substitution.[15]

More recently, both Aq-SET-LRP and RAFT have been used to synthesise block copolymeric arsenicals capable of undergoing simultaneous thermally-induced self-assembly and reductive cross-linking. Considering the reactivity of the pendent As(V)-functional groups present in the block copolymers, two modes of cross-linking have been investigated. Reduction of the pendent As(V)-groups in the presence of hypophosphorus acid (H_3PO_2) and KI affords cross-linking *via* reductive coupling which proceeds with the formation of As-As bonds.[16] The stability of the resulting particles in aqueous solution and 5 mM GSH increases as a function of the AsAm mole ratio whilst under simulated oxidative stress (5 mM, H_2O_2) the particles disassembled irrespective of the AsAm mole ratio. These properties are mirrored by polymeric arsenical hydrogels prepared using the same chemistry.[17] Alternatively, when reductive coupling is performed in the presence of polythiol reagents cross-linking proceeds through the formation more enthalpically favoured As-S bonds.[18] These polymeric arsenical particles are markedly more stable in aqueous solution and 5 mM GSH; crucially the stability (*i.e.* responsivity) towards simulated oxidative stress, can be tuned as a function of the [As] : [SH] and thiol valency of the polythiol cross-linker.

Arsines (As(I)) or cyclic oligoarsines (RAs_n)[19, 20] are interesting functional groups for the development of responsive materials as the oligo-cyclic structures are readily accessible by reduction of the corresponding arsenic acids.[21, 22] The resulting As-As bonds are labile, being prone to homolysis or hydrolysis and oxidation back to As(III) and As(V) respectively. Chujo and co-workers proposed that homolysis of the cyclic oligo-arsines resulted in the formation of arsenic biradicals and employed such structures as co-monomers for ring-collapsed radical alternating copolymerization (RCRAC) with acetylenes to form poly(vinylene arsines).[23] Structurally, the poly(vinylene-arsines) were shown to have a backbone composed of alternating As(III) and vinylene groups in a *trans*-1,2 geometry with a 1 : 1 stoichiometry, irrespective of the initial monomer feed. Crucially, the vinylene-arsine repeating unit was

shown to be resistant to oxidation by peroxides.

Herein, we report the cross-linking of self-assembled polymeric arsenical nanoparticles *via* sequential reductive coupling and RCRAC in the presence of functional acetylenes. The resulting nanoparticles are oxidatively stable and use of propargyl-*O*-rhodamine-B ester during cross-linking provides access to fluorescent nanoparticles which have been used to confirm *in vitro* cell uptake.

EXPERIMENTAL

Materials & Instrumentation

N-(4-(2,2,3,3,7,7,8,8-Octamethyl-1,4,6,9-tetraoxa-5λ^5-arsaspiro[4.4]non-5-yl)-phenyl-2-propenamide) (AsAm(pin$_2$))[15] and 2-((butylthio)-carbonothioyl) thio propanoic acid (PABTC) were synthesised according to the reported literature.[24] *N*-Isopropylacrylamide (NIPAm, 97%) was purchased from sigma and recrystallized in hexane from diethyl ether. Dimethyl 2,2'-azobis(2-methylpropionate) (V601) was purchased from Wako. Potassium Iodide, glutathione (GSH), hydrogen peroxide (30 % w/w), hypophosphorous acid (50% w/w), and poly(ethylene glycol) methyl ether acrylate (PEGA, average M_n = 480 g mol^{-1}) were purchased from Sigma Aldrich and used as received. Membrane dialysis tubing (nMWCO 3.5 kDa) was obtained from Spectrum Laboratories. Nuclear Magnetic Resonance (NMR) spectroscopy (^{1}H NMR) was recorded on a Bruker HD 300 spectrometer (300 MHz) at 27 °C in either deuterated chloroform ($CDCl_3$), dimethyl sulfoxide (δ_6-DMSO) or water (D_2O). Chemical shift values (δ) are reported in ppm. The residual proton signal of the solvent (δ_H = 7.26 ppm for $CDCl_3$, δ_H = 2.50 ppm for DMSO, δ_H = 4.76 ppm for D_2O) was used as internal reference. ACDLABS software was used to analyse the data obtained. Size Exclusion Chromatography (SEC) was conducted using an Agilent 390-LC MDS instrument equipped with differential refractive index (DRI), viscometry (VS), dual angle light scatter (LS) and dual wavelength UV detectors. The system was equipped with 2 x PLgel Mixed D

columns (300 x 7.5 mm) and a PLgel 5 μm guard column. The eluent was DMF containing 5 mmol NH_4BF_4 as an additive. Samples were run at 1 ml/min at 50 °C. Poly(methyl methacrylate) (PMMA) standards (Agilent EasyVials) were used for 3rd order calibration between 2 x 10^2 – 1.0 × 10^6 g mol^{-1}. Analyte samples were filtered through 450 μm nylon filters pore size before injection. $M_{n,SEC}$ and $Đ_m$ values of the synthesized polymers were determined by conventional calibration using Agilent GPC/SEC software. Infrared (IR) spectra were recorded on a Bruker VECTOR-22 FTIR spectrometer using a Golden Gate diamond attenuated total reflection cell. Ultraviolet-visible (UV-Vis) calibration curves for experimental cross-linking density was recorded on an Agilent Technologies Cary 60 UV-Vis at a wavelength of 531 nm using a cuvette with a 1 cm path length and solutions of 1 mg/mL. The fluorescent intensity was monitored using Agilent Technologies Cary Eclipse Fluorescence Spectrophotometer at an excitation wavelength of 553 nm and collection of emission at 627 nm based on rhodamine B using a cuvette with a 1 cm path length and solutions of 1 mg/mL. Hydrodynamic diameters (D_h) and size distributions were determined by Dynamic Light Scattering (DLS) on a MALVERN Zetasizer Nano ZS operating at 25 °C with a 4 mW He-Ne 633 nm laser module. Measurements were made at a detection angle of 173° (back scattering). Measurements were repeated three times with automatic attenuation selection and measurement position. The results were analysed using Malvern DTS 6.20 software. PDI values were calculated using equation Eq 4.1

$$PDI = \frac{\sigma^2}{d^2} \qquad \text{(Eq 1)}$$

Where σ is the standard deviation and d is the diameter both obtained from the number distribution. Atomic Force Microscopy (AFM) images were recorded on a Bruker Dimension Icon instrument operated in peak force tapping mode. The probes used were ScanAsyst silicon tips with a resonance frequency of 70 kHz and a spring constant of 0.4 N m^{-1}. Samples were prepared by drop casting 5 μL of a 1 mg/mL aqueous nanoparticle solution onto a freshly cleaved sheet of mica, left to stand for 30 seconds and dried under of Nitrogen. Transition Electron Microscopy (TEM) samples were prepared by placing

a 400 mesh carbon coated Formvar copper grid onto a 20 µL droplet of aqueous nanoparticles (1 mg/mL) in a petri dish, leaving for 10 minutes prior to drawing off the solution. The grid was then stained by placing onto a 20 µl droplet of aqueous uranyl acetate (0.2 wt%), leaving for 10 minutes before drawing off excess liquid and allowed to air-dry overnight. TEM images were acquired using a JEOL 2100 TEM operating at a 200 kV accelerating voltage. Images were captured using Digital Micrograph® and analysed with ImageJ.

General cell culture

PC3 cells were purchased from ECACC and cultured as single monolayers at 310 K in a humidified atmosphere containing 5% CO_2. Cells were sub-cultured at regular intervals and passages made by trypsinising cells when at 80-90% confluence. Media used was Dulbecco's Modified Eagle Medium (DMEM) supplemented with 10% of foetal calf serum, 1% of L-glutamine and 1% penicillin/streptomycin.

Cell viability

PC3 cells were cultured in High Glucose DMEM medium supplemented with 10% fetal bovine serum. For cell viability evaluation, PC3 cells were seeded in a 96 well plate at a density of 1×10^4 cells per well. After 16 h, the culture medium was replaced by fresh media containing a series of dilution of the polymers (0.0625, 0.125, 0.25, 0.5, 1 and 2 mg/mL), prepared from stock solutions in PBS at 500 µM. Following 24 h incubation, the medium was removed and replaced with fresh medium. The cells were incubated with a freshly prepared solution of XTT (0.2 mg/mL) and *N*-methyl dibenzopyrazine methyl sulfate (250 µM) in medium for 16 h. Absorbance of the samples was finally measured using a plate reader at 450 nm and 650 nm. The data presented are representative of a minimum of two independent experiments where each sample was measured in triplicate. Errors reported correspond to the SD of the mean.

Cell uptake

PC3 Cells were seeded into a black 96 imaging well plate with a clear bottom at a density of 5000 cells per well and allowed to grow for 24 h. The culture medium was replaced with media containing rhodamine labelled nanoparticles (100 µg/mL) 2 h and 24 h prior to imaging. Cellular fluorescence was measured using a Cytation 3 Cell Imaging Multi-Mode ReaderTM from Biotek®, with quantification from the Gen5TM software. Single cells were isolated using the blue channel (Hoechst 33258) using a secondary mask with an area of 12 µm. Following background reduction using a roll ball model (25 µm), fluorescence associated with rhodamine (RFP filter, λ_{ex} = 531 nm, λ_{em} = 593 nm) was assigned as intracellular fluorescence. To compensate for the varying molar content of Rhodamine B during the NP cellular uptake studies, the internalisation values were normalised based on the relative fluorescence intensity of each particle. The normalisation factors were calculated from the gradients of the linear regions of concentration/ fluorescence intensity curves measured from 5 – 50 µg mL-1 at the wavelengths used to monitor cellular uptake (**Fig. S17**). Raw intracellular fluorescence was multiplied by the normalisation value for comparison. This correction has been added to the SI in **Table S4**. Data is represented as the arithmetic mean ± SD with experiments conducted in triplicates.

Confocal microscopy

7500 PC3 cells were seeded in a 10 well microscopy slide and left to incubate for 24 h, at 37°C in 5% CO_2 atmosphere. The culture medium was replaced with media containing nanoparticles (100 µg/mL) and incubated for 24 h prior to imaging. Cells were stained with 1) Nuclear stain – Hoechst 33258 (0.5 µg/mL; 30 min), 2) Lysotracker-Green (100 nM; 2 h), 3) Mitotracker green (100 nM; 30 min). Immediately prior to imaging, the cells were washed with PBS 3x and finally the media replaced with 100 µL of phenol red free DMEM. Cells were imaged with a Zeiss 880 confocal microscope using a 40 x objective, at 37°C with the following laser settings: 1) Hoechst dye (blue channel), 405 nm laser, 420-

500 nm emission band. 2) Lysotracker and Mitotracker (green channels), 488 nm laser 500-550 nm emission band. 3) rhodamine labelled compounds and free rhodamine B (red channel), 561 nm laser (570-630 nm emission band). Images were processed with Fiji software.

Synthetic methods

Spectroscopic, chromatographic and microscopy data can be found in the SI.

General procedure for synthesis of PEGA$_{20}$-*b*-[NIPAM$_{80-n}$-*st*-AsAm$_n$] by RAFT, P1 – P4

2-(((Butylthio)carbonothioyl)thio)propanoic acid (PABTC-C4, 24.8 mg, 0.1 mmol), PEGA$_{480}$ (1 g, 2.1 mmol) and 2,2'-azobis(2-methylpropionate) (V601, 1.44 mg, 6.3 μmol) were combined in a vial with 2,2,2-trifluoroethanol (TFE, 1094 μl total volume) and deoxygenated by sparging with N_2 for 15 min. Samples were taken before placing in an oil bath at 65 °C for 16 h and again upon completion for ^{1}H NMR and SEC. Chain extension of the macro-RAFT agent was performed *in-situ via* addition of deoxygenated mixtures of *N*-isopropylacrylamide (NIPAM, 80-n eq), AsAm(pin$_2$) (n eq), in varying feed ratios, and V601 (0.69 mg) in TFE (1,649 μl total volume). Samples were again taken before placing in an oil bath at 65 °C for 16 h and again upon completion for ^{1}H NMR and SEC. The diblock copolymers were then dialysed (nMWCO 3.5 kDa) against dilute hydrochloric acid (HCl, 0.1 M) for 24 h, then deionised water for a further 24 h to ensure complete removal of the pinacol protecting group from AsAm(pin$_2$) yielding the desired AsAm-functional block copolymers. The purified products were isolated by lyophilisation.

Propargyl-*O*-rhodamine B ester[25]

Rhodamine B (1 eq), DCC (1.5 eq), DMAP (0.2 eq) were dissolved in anhydrous DCM (50 ml) and stirred for 30 min. Propargyl alcohol (1.5 eq) was added and stirred at room temperature for 16 h. The crude product was purified by flash column in 1% methanol in DCM, the resulting product fractions combined and the solvent removed in vacuo to yield iridescent black crystals (57% yield). ^{1}H NMR (400

MHz, $CDCl_3$, 298 K) δ = 8.30 (d, J_{HH} = 7.2 Hz, 1H, H_i), 7.84 (dd, J_{HH} = 7.2, 7.3 Hz, 1H, H_g), 7.75 (dd, J_{HH} = 7.9, 7.3 Hz, 1H, H_h), 7.31 (d, J_{HH} = 7.9 Hz, 1H, H_f) 7.06 (d, J_{HH} = 9.5 Hz, 2H, H_e), 6.90 (d, J_{HH} = 9.7 Hz, 2H, H_d) 6.80 (s, 2H, H_c) 4.60 (s, 2H, H_j) 3.63 (q, J_{HH} = 13.3, 6.4 Hz, 8H, H_b) 2.40 (s, 1H, H_k) 1.30 (t, J_{HH} = 6.8, 12H, H_a); ^{13}C NMR (400 MHz, $CDCl_3$ 298 K) δ = 164.2, 75.6, 52.9, 46.2, 12.7,; LR-MS (ESI, +ve) *m/z* ($C_{31}H_{34}N_2O_3$); expected 481.2, obtained 481.4 ($[M+H]^+$).

General procedure for the self-assembly and cross-linking of PEGA$_{20}$-*b*-[NIPAm$_{80-n}$-*st*-AsAm$_n$] *via* sequential reductive coupling and RCRAC

As-functional polymers (**P1** – **P4**) were dissolved in a deoxygenated solution of aqueous hypophosphorus acid (H_3PO_2, 10 wt%, 10 mg/mL polymer) and deoxygenated KI (1 vol% from a 3 wt% aq solution) was added. The solution was heated at 60 °C for 30 min. The functionalized acetylene (2.5 eq. w.r.t. [As]) and VA-044 (0.1 eq w.r.t [As]) were separately dissolved in HPLC grade H_2O and sparged with N_2 before addition to the hot polymer solutions, which were heated for a further 16 h. The resulting solutions were dialysed (nMWCO 3.5 KDa) against deionised water for 24 h and the crosslinked particles isolated by lyophilisation. The resulting solutions of functionalised nanoparticles were purified by aqueous dialysis (nMWCO 3.5 KDa) to removed unreacted acetylenes. The purified particles were isolated by lyophilisation.

General procedure for particle stability

Polymer nanoparticles were dissolved separately in deionised water, aqueous glutathione (5 mM) and aqueous H_2O_2 (5 mM) (1 mg/mL). The solutions were filtered through (450 μm nylon filters) into separate plastic cuvettes (with a lid) and incubated at 37 ^{0}C in a water bath. Disassembly was monitored through the measurement of changes in D_h as a function of time by DLS.

RESULTS AND DISCUSSION

Synthesis of thermoresponsive PEGA$_{20}$-*b*-[NIPAm$_{80-n}$-*st*-AsAm$_n$] scaffolds. Initially, thermoresponsive block copolymers composed of a corona-forming poly(ethylene glycol) methyl ether acrylate (PEGA, M_n = 480 gmol^{-1}) block and a core-forming *N*-isopropylacrylamide (NIPAm) block were synthesized using RAFT. In order to investigate vinylene-arsine cross-linking, AsAm was incorporated into the core-forming block at various mole ratios; targeting polymers with final compositions of P(PEGA$_{20}$-*b*-[NIPAm$_{80-n}$-*co*-AsAm$_n$]) (**P1**, n = 5; **P2**, n = 10; **P3**, n = 15; **P4**, n = 20). Detailed discussion of the synthesis of the organic arsenic acrylamide monomer, (*N*-(4-(2,2,3,3,7,7,8,8-octamethyl-1,4,6,9-tetraoxa-5λ^5-arsaspiro[4.4]non-5-yl)-phenyl-2-propenamide; AsAm(pin)$_2$) and subsequent polymerizations are reported in our previous work. [15, 18] This was repeated here with the initial PEGA$_{480}$ block (targeting DP$_n$ = 20) synthesized using 2-((butylthio)-carbonothioyl) thio propanoic acid (PABTC) as the RAFT agent, V601 as initiator and trifluoroethanol (TFE) as the solvent at 65 °C ([PEGA$_{480}$] = 1 M; [CTA]$_0$ / [V601]$_0$ = 50). The corona-forming PEGA$_{480}$ blocks were obtained in high conversions (> 99%) with DP$_n$ = 23 – 27, according to ^{1}H NMR, close to the targeted DP$_n$ = 20. Size exclusion chromatography revealed well-defined peaks with good agreement between theoretical and experimental number average molecular weights ($M_{n,\mathrm{th}}$ = 11300 - 13200 gmol^{-1}; $M_{n,\mathrm{SEC}}$ = 8400 - 10400 gmol^{-1}) and low dispersities ($Đ_m$ = 1.16 - 1.27) (**Table 1**, **Fig. S2**).

Table 1. Arsenic functional block copolymers synthesized by RAFT. Monomer conversion determined by ^{1}H NMR of protected polymer in $CDCl_3$. SEC carried out using DMF as an eluent.

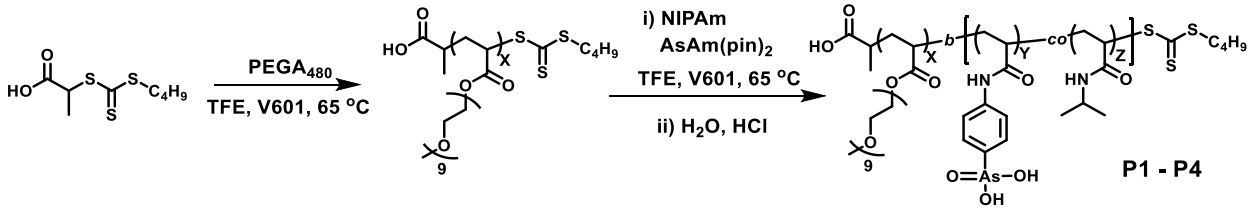

Polymer Composition	Protected polymer (step i)				After deprotection (step ii)		
	Con.	$M_{n,th}$ (g mol^{-1})	$M_{n,SEC}$ (g mol^{-1})	$Đ_m$	$M_{n,th}$ (g mol^{-1})	$M_{n,SEC}$ (g mol^{-1})	$Đ_m$

	P[PEGA$_{23}$]	> 99%	11300	9400	1.23			
P1	P[PEGA$_{23}$ -*b*-(NIPAm$_{73}$-*co*-AsAm$_{4}$)]	> 99%	21800	17500	1.27	21200	13900	1.33
	P[PEGA$_{27}$]	> 99%	13200	10400	1.27			
P2	P[PEGA$_{27}$ -*b*-(NIPAm$_{80}$-*co*-AsAm$_{11}$)]	> 99%	21800	22000	1.40	25400	10500	1.53
	P[PEGA$_{23}$]	> 99%	11300	8400	1.23			
P3	P[PEGA$_{23}$ -*b*-(NIPAm$_{66}$- *co*-AsAm$_{15}$)]	> 99%	25500	21000	1.25	23100	9900	1.44
	P[PEGA$_{24}$]	> 99%	11800	8700	1.16			
P4	P[PEGA$_{24}$ -*b*-(NIPAm$_{56}$- *co*-AsAm$_{18}$)]	> 99%	26300	21300	1.27	23300	10200	1.19

Chain extension was achieved upon *in-situ* addition of varying amounts of AsAm(pin)$_2$ and NIPAm (targeting overall DP$_n$ = 80) to the polymerization solution containing the PEGA$_{480}$ macro-CTA. High conversions were again obtained (> 99%), and efficient re-initiation from the PEGA$_{480}$ macro-CTA was confirmed by SEC through clear shift in the molecular weight ($M_{n,\mathrm{SEC}}$ = 17500 - 22000 gmol^{-1}) with retention of relative low dispersities ($Đ_{\mathrm{m}}$ = 1.25 - 1.40) (**Table 1**, **Fig. S2**). To obtain the desired, reactive, As(V) functional group, the AsAm(pin)$_2$ pendent group was deprotected during acidic dialysis of the polymer scaffolds to yield pure As(V)-functional block copolymers **P1** – **P4** with increasing incorporation of AsAm (DP$_{n,\mathrm{th}}$ = 5 – 20; DP$_{n,\mathrm{NMR}}$ = 4 – 18).

Self-assembly and cross-linking of PEGA$_{20}$-*b*-[NIPAm$_{80-n}$-*st*-AsAm$_n$] *via* reductive coupling. To confirm that the As(V)-functional block copolymers were thermoresponsive and capable of undergoing self-assembly, as previously observed, variable temperature dynamic light scattering (DLS) in aqueous solution was performed (1 mg/mL). As expected, at 25 °C the block copolymers are fully soluble and small, unimeric, hydrodynamic diameters (D_{h} = 2.1 – 3.1 nm) were obtained. Upon heating to 60 °C, to promote the phase transition and insolubility of the NIPAm-containing block, D_{h} increased to 14 – 20 nm, indicative of self-assembly into a higher order structure (**Fig. S3**). Likewise, to confirm that the AsAm groups were present and available for further reaction, **P1** – **P4** were heated in the presence of H_3PO_2 and KI to stimulate cross-linking through the formation of As-As bonds *via* reductive coupling.

The nanoparticles derived from **P1** (**$NP_{As(I)-4}$**) were found to be unstable, undergoing disassembly during aqueous dialysis. However, the nanoparticles derived from **P2** – **P4** (**$NP_{As(I)-11}$**, **$NP_{As(I)-15}$**, **$NP_{As(I)-18}$**), with $DP_{n,AsAm} \geq 10$, retained their self-assembled structures during and post purification (**Fig. S4**). The morphology of the stabilized nanoparticles was characterized by using atomic force microscopy (AFM) and transition electron microscopy (TEM) of **$NP_{As(I)-18}$** which confirmed the formation of nanoparticles with sizes < 25 nm (**Fig. S5**). This data is consistent with our previous work in which the stability of **$NP_{As(I)-n}$** was directly related to the mole fraction of the AsAm in the parent polymer *i.e.* **P4** > **P3** > **P2** > **P1**.[16]

Self-assembly and cross-linking of $PEGA_{20}$-*b*-[$NIPAm_{80-n}$-*st*-$AsAm_n$] *via* sequential reductive coupling and RCRAC. In the work of Chujo *et al*,[23, 26-32] the formation of poly(vinylene arsines) was proposed to proceeded *via* a RCRAC mechanism initiated by thermal decomposition of a radical initiator (2,2'-azobisisobutyronitrile, AIBN) to promote the homolysis of labile As-As bonds in organic solvents (benzene) resulting in the formation of As-biradicals. These reactive biradical intermediates can either recombine to reform labile As-As bonds, or they can add to acetylene (or vinyl)[33, 34] monomers leading to the formation of a new As-C bond and a reactive vinyl radical during the rate determining step. The vinyl radical then rapidly reacts with As-As or other As-(bi)radicals resulting in the formation of another As-C bond.

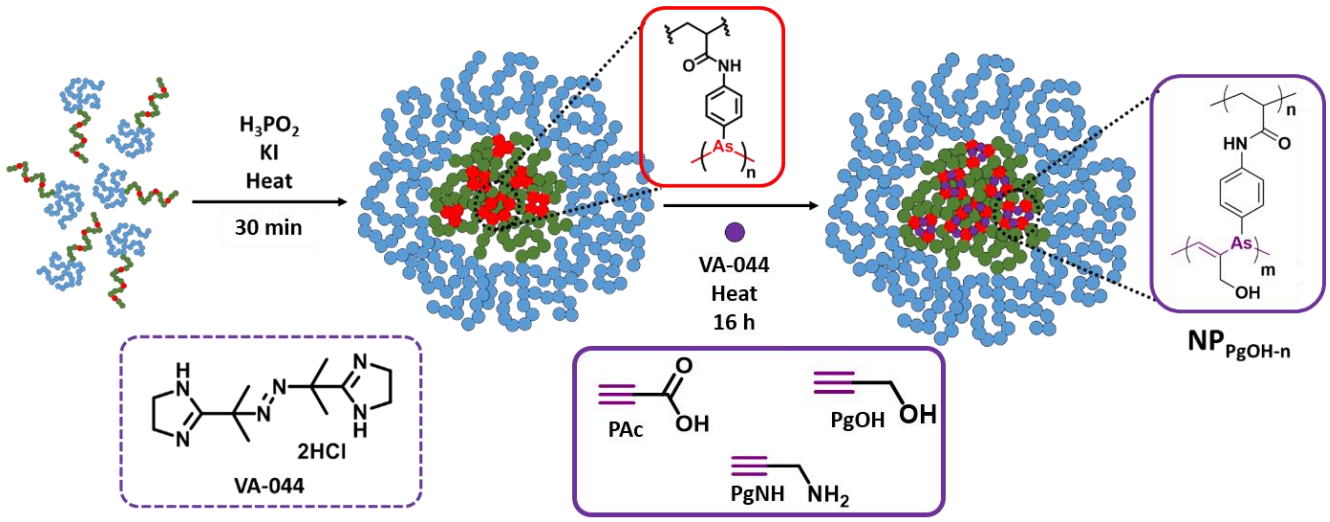

Scheme 1. Schematic representation of the self-assembly and cross-linking of polymer **P1** – **P4** through *in-situ* reductive coupling and RCRAC of As(I). The As(I) cross-linked nanoparticles are initially generated under elevated temperature in the presence of H_3PO_2 and KI to promote reductive coupling of the As(V) pendent groups before the addition of VA-044 and water soluble acetylenes to promote vinylene-arsine formation *via* RCRAC.

Inspired by this, we hypothesized that performing sequential reductive coupling and RCRAC *in-situ*, by feeding in a mixture of a water soluble azo-initiator and water soluble acetylene to the **NP$_{As(I)-n}$** solutions at 60 °C would promote further reaction and cross-linking *via* the formation of vinylene-arsine bonds (**NP$_{V-As}$**). 2,2'-Azobis[2-(2-imidazolin-2-yl)propane]dihydrochloride (VA-044) was identified as a suitable initiator and propargyl alcohol (PgOH), propargyl amine (PgNH) and propiolic acid (PAc) were selected as the acetylenes due to their water solubility and varying functionality (**Scheme 1**). Initially, polymers **P1** – **P4** were investigated using VA-044 and propargyl alcohol to promote further cross-linking. A deoxygenated mixture of these reagents was added after 30 minutes of initial reductive coupling, to form **NP$_{As(I)-n}$** *in-situ* and then left for 16 h at 60 ºC. After extensive purification by aqueous dialysis, the nanoparticles were initially characterised by infra-red (IR) spectroscopy with changes in the region between 1000 – 750 cm^{-1}, corresponding to the As-O bond signals, confirming the reduction of the pendant arsenic acid (As(V)) groups (**Fig. 1**). Furthermore, the broad signal (3700 - 2500 cm^{-1}) present in the parent scaffold **P4**, attributed to the O-H groups of arsenic acid group decreased.

Incorporation of the propargyl alcohol was indicated by increase in the O-H signal at 3450 cm^{-1}, whilst the absence of strong alkyne stretches at ~ 3300 cm^{-1} and 2100 cm^{-1} provide indirect evidence for incorporation via vinylene-arsine bond formation (*vide infra*).

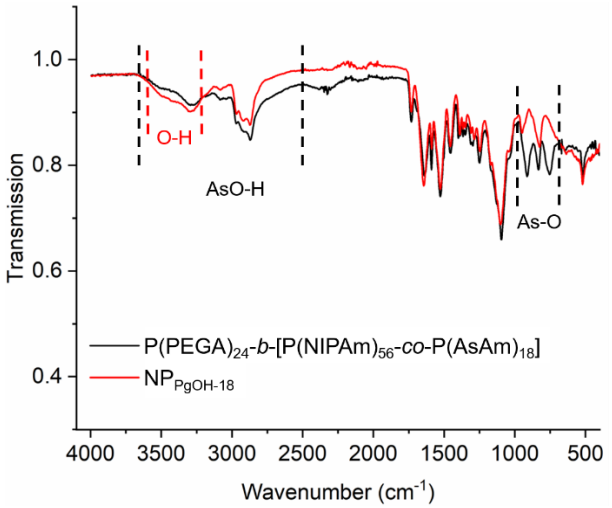

Fig. 1. Infrared spectra of **P4** (black) and **NP$_{PgOH-18}$** (red) indicating reduction and modification of the pendent arsenic acid (As(V)) groups via changes in the O-H and As-O regions.

Characterisation by DLS (1 mg/mL, H_2O) revealed the presence of stable nanoparticles (**NP$_{PgOH-n}$;** n = 4, 11, 15, 18) at 25 °C (D_h = 10.7 – 16.8 nm) and 60 °C (D_h = 9.5 – 14.5 nm **Table S1**, **Fig. 2A**). The nanoparticles exhibited mild thermoresponsive character due to the presence of PNIPAm in the core-forming block. Small contractions in the hydrodynamic volume upon heating apparent in the number distribution plots (**Fig. 2A**) were supported by reductions in size according to the intensity distribution and correlation coefficient plots (**Fig. S6**). The morphology of the nanoparticles was assessed *via* TEM and AFM using **NP$_{PgOH-18}$**, revealing the formation of spherical nanoparticles with sizes < 35 nm (**Fig. 2B & 2C**).

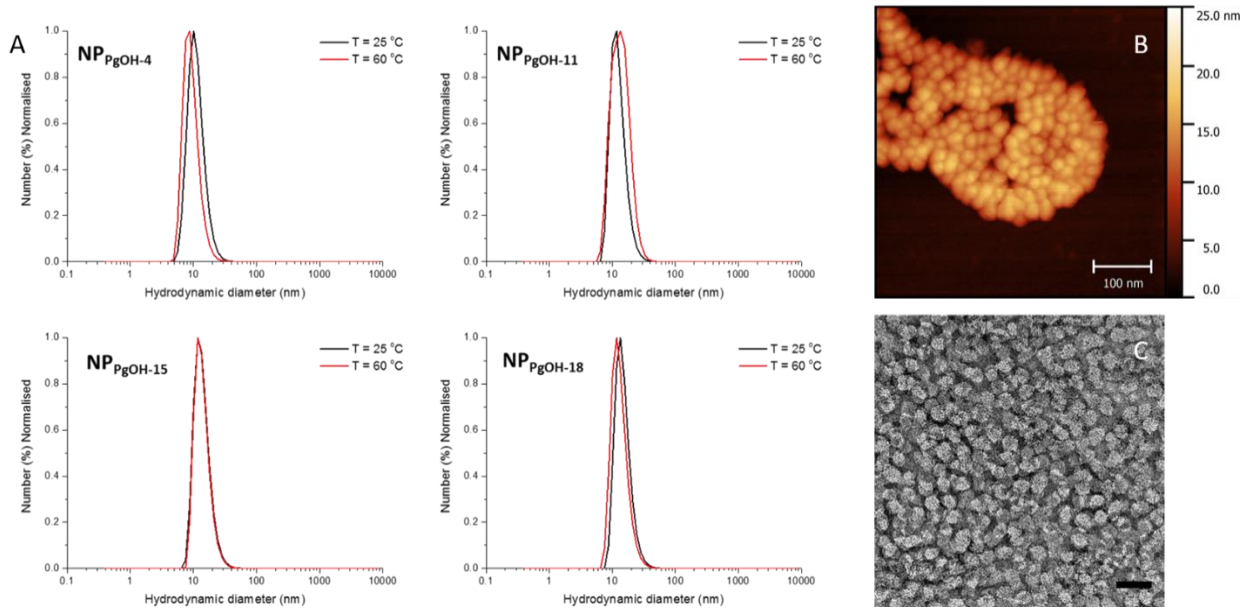

Fig. 2. (A) Particle size distribution curves of **NP$_{PgOH-n}$** (n = 4, 11, 15, 18) by DLS (1 mg/mL, H_2O) analysis at 25 °C and 60 °C; (B) AFM and (C) TEM of **NP$_{PgOH-18}$** (scale bar = 100 nm)

The proposed stability of the **NP$_{PgOH-n}$** particles is in contrast to the nanoparticles formed by reductive coupling alone; of which **NP$_{As(I)-4}$** was not sufficiently stable, disassembling during purification (**Fig. S4**). We hypothesize that the increased stability is due to the formation vinylene-arsine bonds between polymer chains which elicits an increased inertia towards oxidation and results in the formation of As-C bonds, which are stronger than As-As bonds and further stabilized through n_{As}-π_C conjugation.[35] The relative stability of **NP$_{PgOH-n}$** was further investigated under model biological redox conditions *i.e.* in the presence of reduced glutathione ([GSH] = 5 mM) and hydrogen peroxide ([H_2O_2] = 5 mM) at 37 °C. Redox and reactive oxygen species (ROS) responsive materials are promising candidates for nanomedicine based on the concentration gradient between healthy and diseased (e.g. tumours) tissues.[36, 37] For example, the extracellular concentration of GSH ranges between 2-20 μM whilst the intracellular concentration can reach 10 mM, which can increase 4-fold in tumour tissues.[38] Likewise, the concentration of H_2O_2 is regulated at 20 nM in healthy cells, whilst in tumour cells, overproduction and retention can lead to concentrations up to 100 μM.[39] Considering the redox reactivity of arsenicals, we have previously reported that in the presence of GSH or H_2O_2, nanoparticles cross-linked *via* As-S bonds

(**NP$_{As-S}$**) exhibited greater stability than those cross-linked *via* As-As bonds (**NP$_{As(I)-n}$**) and in both cases the stability can be related to the AsAm mole ratio present in the parent polymers.[18] Here, all **NP$_{PgOH-n}$** particles, including **NP$_{PgOH-4}$**, were stable over the course of the experiment (7 days) in both GSH and H_2O_2 at intracellular and exaggerated intracellular concentrations respectively (**Fig. 3**). The enhanced stability of **NP$_{PgOH-n}$** reflects the stability of the vinylene-arsine bonds proposed to constitute cross-linking. In particular, the resilience to oxidation by H_2O_2 is in agreement with our hypothesis and the work of Chujo *et al*, in which poly(vinylene-arsines) were found to be resistant to oxidation by H_2O_2.[23]

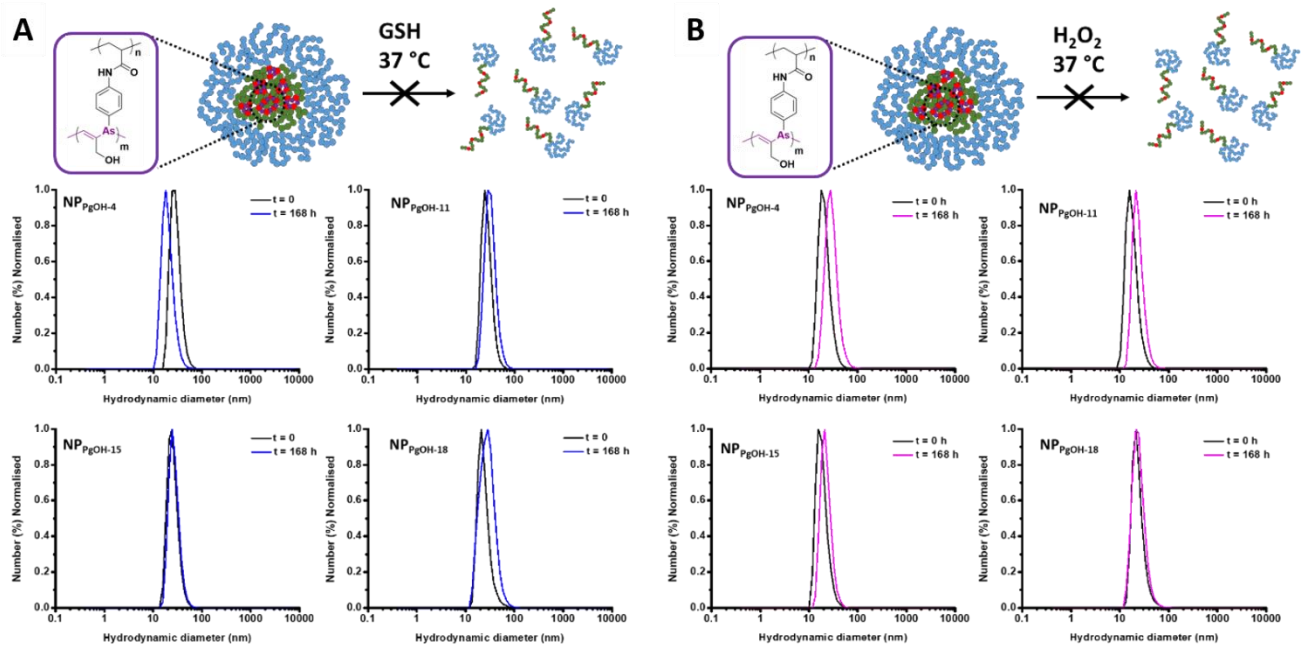

Fig. 3. Particle size distribution curves of **NP$_{PgOH-n}$** (n = 4, 11, 15, 18) by DLS (1 mg/ml, H_2O) as function of time in (A) aqueous GSH (5 mM) and (B) H_2O_2 (5 mM).

To demonstrate the versatility of the RCRAC method, other functional water soluble alkynes were examined as co-monomers for cross-linking. Given the mechanism of RCRAC, it was hypothesized that there would be orthogonality with functional groups such as amines and carboxylic acids. Propargyl amine and propiolic acid were therefore employed as the acetylene monomers, yielding stabilised nanoparticles **NP$_{PgNH-n}$** and **NP$_{PAc-n}$** (n = 11, 15, 18) respectively from **P2** – **P4** (D_h = 12.7 – 30.9 nm,

Table S2, **Fig. S7-S8**). Changes in the IR spectra in the region corresponding to the As-O bond signals (1000 – 750 cm^{-1}) again indicated reduction and modification of the pendant arsenic acid (As(V)) groups (**Fig. S9**). Characterization of **$NP_{PgNH-18}$** and **NP_{PAc-18}** by TEM and AFM confirmed the formation of nanoparticles with similar size and morphology compared to **$NP_{PgOH-18}$** (**Fig. S10-S11**). The stability of **NP_{PgNH-n}** and **NP_{PAc-n}** in GSH and H_2O_2 was identical to **NP_{PgOH-n}** with self-assembled structures retained over the course of the 7-day experiment (**Fig. S12-S13**).

Cell viability of NP_{V-As}. With potential biomedical applications in mind, and considering the chemical reactivity and biochemical activity of (in)organic arsenicals, it is critical to evaluate the cytotoxicity of all of the polymeric arsenicals and nanoparticles synthesized. Therefore, for purposes of screening and to be consistent with our previous work, the acute toxicity of the parent polymeric arsenicals (**P1 - P4**) and all subsequently formed nanoparticles (**NP_{PgOH-n}**, **NP_{PAc-n}**, and **NP_{PgNH-n}**) was determined *in vitro via* a standard XTT assay using the Prostate carcinoma cell line (PC3) as a model. The polymers and corresponding nanoparticles were non-toxic up to the maximum concentration that was tested (2 mg/mL) (**Fig. 4**), which was consistent with our previous results.[14-18]

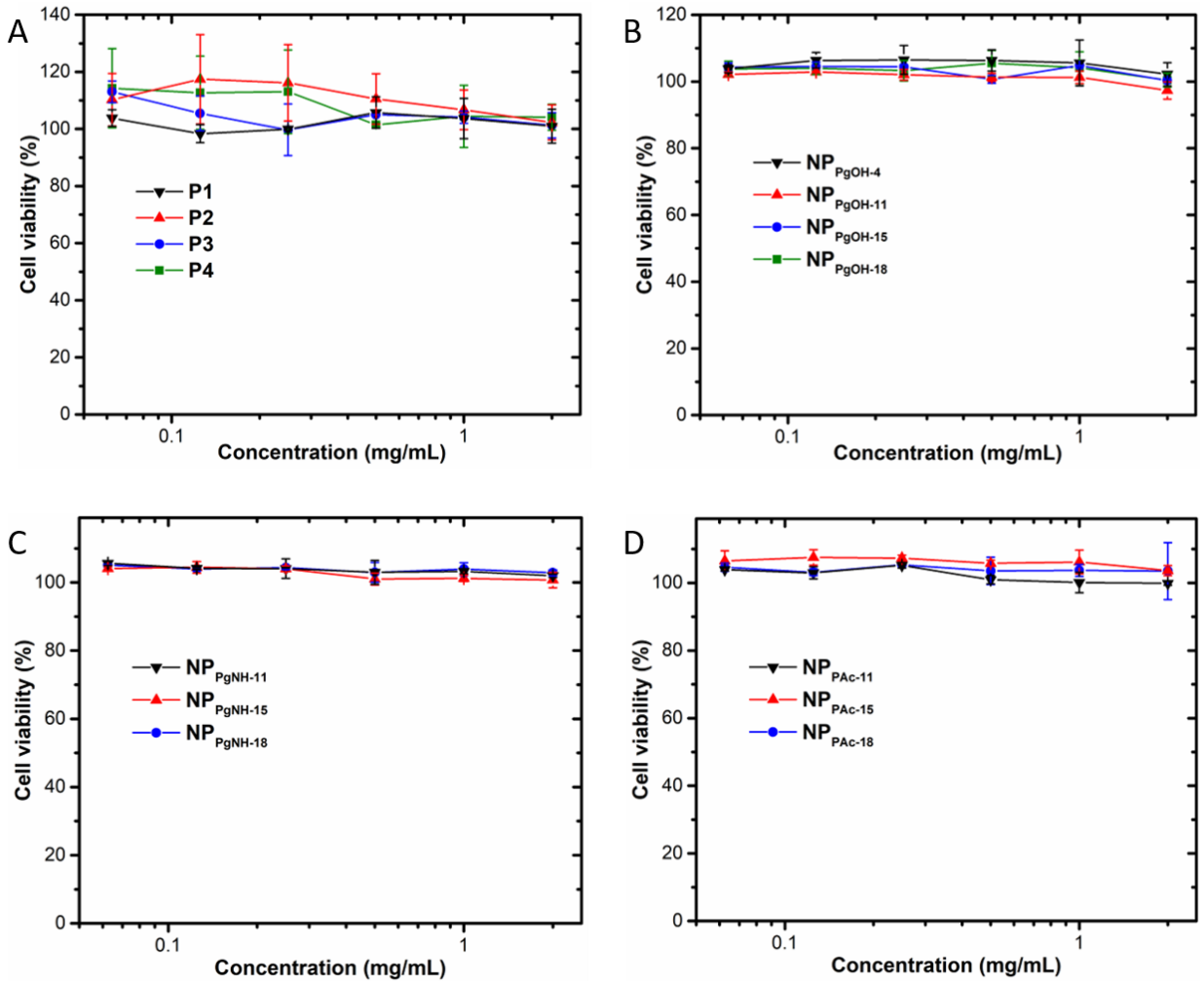

Fig. 4. In vitro cell viability of (A) **P1 - P4**; (B) **NP$_{PgOH-n}$**; (C) **NP$_{PgNH-n}$** and (D) **NP$_{PAc-n}$** using XTT viability assay with PC3 cell line.

Preparation of fluorescent NP$_{V-As}$ using propargyl-*O*-rhodamine ester. The cell viability results are promising and in agreement with evaluation of related polymeric arsenical scaffolds and nanoparticles. However, it is not yet known whether the nanoparticles are taken up by the cells and if they are, how they are distributed through the cell *in vitro*. The sequential reductive coupling - RCRAC method offers the potential to introduce functionality suitable for cellular imaging into the nanoparticles. Rhodamine B was selected as a cheap water soluble fluorescent probe and an *O*-propargyl-ester derivative of rhodamine B was synthesized under standard Steglich esterification conditions using propargyl alcohol (**Fig. S14**).[25] The RCRAC method was then employed to prepare fluorescent nanoparticles (**NP$_{Rh-n}$**) using **P1 - P4** and

propargyl-*O*-rhodamine B ester as the acetylene monomer. Initially, successful loading of the particles with the rhodamine alkyne was confirmed by IR and ^{1}H NMR. Changes in the region corresponding to the As-O bond signals (1000 – 750 cm^{-1}) indicated reduction and modification of the pendant arsenic acid (As(V)) groups (**Fig. 5A**), while the presence of multiple aromatic signals at 7.00 – 8.25 ppm can be attributed to incorporation of the *O*-propargyl-ester derivative of rhodamine B (**Fig. 5B**). Unfortunately, due to the to the expect vinyl proton arising from vinylene-arsine bond formation and other key polymer side-chain peaks in the NMR spectra being obscured it was not possible to quantify the extent of rhodamine incorporation by NMR in d_6-DMSO. Further attempts to quantifiably detect the vinyl proton arising from vinylene-arsine bond formation in D_2O and $CDCl_3$ were also unsuccessful with the proposed vinyl signal at 6.86 and 6.54 ppm respectively obscured by overlap with the broad aromatic region (**Fig S15)**.

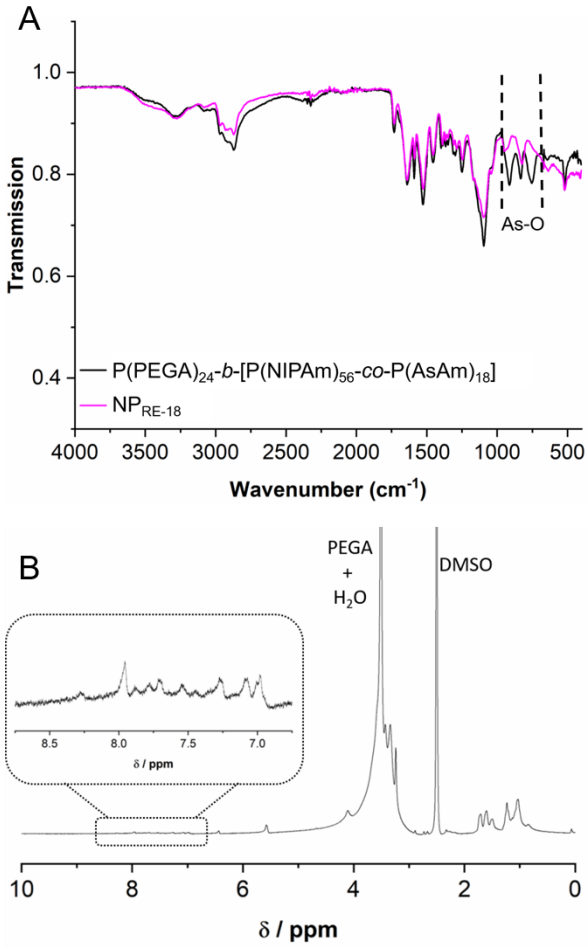

Fig. 5. (A) Infrared spectra of **P4** (black) and **NP$_{RE-18}$** (purple) indicating reduction and modification of the pendent arsenic acid (As(V)) groups via changes in the As-O region. (B) ^{1}H NMR and zoomed inset (d_6-DMSO, 400 MHz, 50 mg/mL) showing incorporation of the rhodamine B *O*-propargyl-ester in **NP$_{RE-18}$.**

Pleasingly, the **NP$_{Rh-n}$** obtained were found to be stable at 25 °C with comparable sizes (D_h = 16.3– 26.7 nm) and morphologies to **NP$_{PgOH-n}$**, **NP$_{PAc-n}$**, and **NP$_{PgNH-n}$** according to characterization by DLS (**Fig. 6A, Fig. S16, Table S3**), AFM (**Fig. 6C**) and TEM (**Fig. 6D**) respectively. Likewise, the stability of **NP$_{Rh-n}$** in GSH and H_2O_2 was identical to **NP$_{PgOH-n}$** with self-assembled structures retained over 7 days (**Fig. S17**). Most significantly, the nanoparticles were also shown to be fluorescent using fluorescence spectroscopy (λ_{ex} = 553 nm; λ_{em} = 617 nm), confirming successful loading with the rhodamine (**Fig. 6B**). Fluorescence measurements of rhodamine-B (acid) revealed excitation and emission wavelengths of λ_{ex} = 554 nm and λ_{em} = 584 nm, whilst propargyl-*O*-rhodamine B ester gave excitation and emission wavelengths of λ_{ex} = 565 nm and λ_{em} = 595 nm. In order to verify that the propargyl-*O*-rhodamine B

ester had been incorporated into the nanoparticles, and to investigate whether any hydrolysis of the ester occurred under the acidic conditions imposed during cross-linking, an ^{1}H NMR experiment in which the propargyl-*O*-rhodamine B ester was subjected to the cross-linking reaction conditions (H_3PO_2, KI, 60 °C, overnight) was performed. Comparison of the spectra at t = 0 and after heating overnight revealed identical structures suggesting that no detectable hydrolysis occurred during the course of the cross-linking (**Fig. S18**).

Based on the proposed 1 : 1 stoichiometry of acetylene and arsenic in poly(vinylene-arsines) and using ultraviolet-visible (UV-Vis) spectroscopy, by extrapolating the concentration from a calibration graph of propargyl-*O*-rhodamine B ester (**Fig. S19**), the degree of cross-linking in **NP$_{Rh-n}$** was semi-quantitatively determined to be between 7 – 32 %. This corresponds to between 1 and 2 AsAm groups per polymer chain reacting to the form the vinylene-arsine cross-links, which is low considering the observed enhancement in stability relative to **NP$_{As(I)}$**. The low level of cross-linking can be attributed to the structure of the acetylenes employed for the RCRAC reaction. During the investigations of the synthesis of linear poly(vinylene-arsines) it was recognized that aromatic acetylenes (e.g. phenylacetylene) were better monomers for RCRAC than aliphatic acetylenes, with the increased relative stability of the vinyl radical adjacent to the aromatic ring proposed to the promote the polymerisation.[28] The acetylenes employed in this work will form relatively less stable vinyl radicals (than aromatic acetylenes). Therefore, although the reaction proceeds enough for cross-linking to be achieved, the overall efficiency is low.

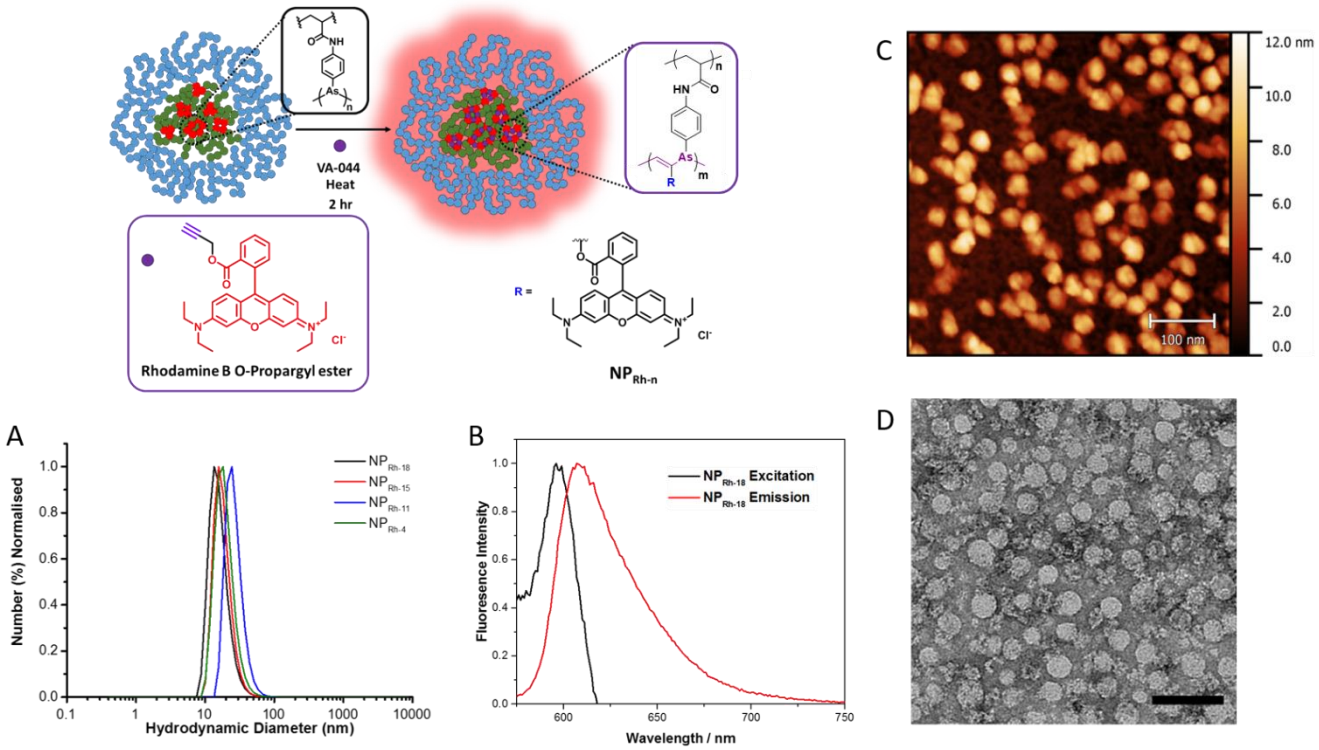

Fig. 6. Schematic representation of the cross-linking of **P1** – **P4** using propargyl-*O*-rhodamine B ester to generate fluorescent nanoparticles nanoparticles, **NP$_{Rh-n}$** (n = 4, 11, 15, 18). (A) Particle size distribution curves by DLS (1 mg/mL); (B) fluorescence spectrum of **NP$_{Rh-18}$** (λ_{Ex} = 553 nm, λ_{Em} = 627 nm); (C) AFM and (D) TEM of **NP$_{Rh-18}$** (scale bar = 100 nm).

The propargyl-*O*-rhodamine B ester functionalised nanoparticles were investigated as models for loading and release of active compounds into the polymeric arsenical nanoparticles. Thus, comparative rates of hydrolysis from rhodamine-loaded particles **NP$_{RE-18}$** (1 mg/mL in phosphate buffer solution (PBS)) were determined *via* dialysis experiments performed at pH = 10.0 (0.01 M sodium hydroxide); 7.0 (PBS); and 5.0 (0.01 M acetic acid); monitoring release by fluorescence measurements on aliquots of the dialysis media (**Fig**. **7**). Under neutral (pH = 7.0) and mildly acidic (pH = 5.0) conditions very little release was observed over course of the experiment (7 days). However, under basic conditions (pH = 10.0), after a lag period of ~ 30 hours, significant hydrolysis was observed. Although, hydrolysis was not observed in a more physiologically relevant pH range, hydrolysis of the propargyl-*O*-rhodamine B ester bond indirectly confirms loading of rhodamine and alludes to the potential to load and release active compounds into the polymeric arsenical nanoparticles using the RCRAC approach, which has not

previously been demonstrated.

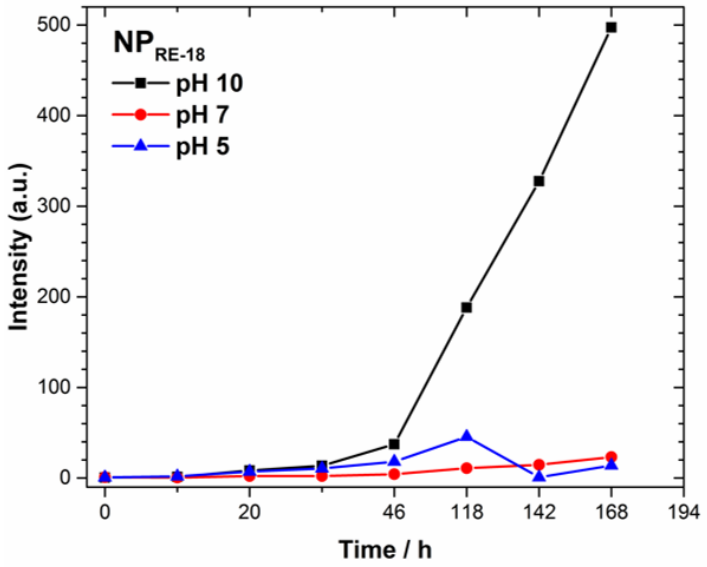

Fig. 7. Fluorescence intensity measurements taken during dialysis of **NP$_{RE-18}$** (1 mg/mL) in a variety of aqueous solutions to correlating to the rate of hydrolysis of rhodamine-*O*-propargyl-ester bond with solution pH.

Cell uptake and co-localization of NP$_{Rh-n}$. PC3 cells were selected as the model cell line for uptake considering their use in viability assays during this and previous work. This would help determine whether the low toxicity of the particles was related to the particle composition/structure or an artefact of a lack of internalisation. Prior to cellular uptake studies, fluorescence normalisation correction curves were plotted for each **NP$_{Rh-n}$** in order to normalise the intracellular fluorescence with the intrinsic particle fluorescence to quantify the relative uptake (**Fig. S20, Table S4**). Subsequently, an increased intracellular fluorescence indicated that cell uptake had occurred after 2 hours of incubation with the **NP$_{Rh-n}$** (**Fig. S21**) and uptake did not increase with longer incubation times e.g. 24 hours (**Fig. S22**). This suggests that the reported cell viability is a result of intrinsic low toxicity of the nanoparticles against PC3 cells, as opposed to evasion from cellular uptake. Increased cellular uptake was observed with increasing mole ratios of AsAm in the parent polymers (**P1** – **P4**) with **NP$_{Rh-18}$** and **NP$_{Rh-15}$** showing higher uptake than **NP$_{Rh-11}$** and **NP $_{Rh-4}$** (**Fig. 8**). The size, shape and stability of nanoparticles is known to have an impact

on cellular uptake.[40-44] However, the nanoparticles fabricated during this work all have similar size and shape, with spherical nanoparticles of sizes < 35 nm being isolated, which are the ideal shape and size for *in vivo* tumour accumulation.[45-47] The only notable difference between the particles formed is the mole ratio of AsAm, which increases in the parent polymers from **P1** – **P4**. This alludes to potential targeting or stimulation of uptake (*e.g.* thiol-mediated)[48, 49] conferred by the presence of the arsenic in the nanoparticle composition; work is ongoing to investigate this.

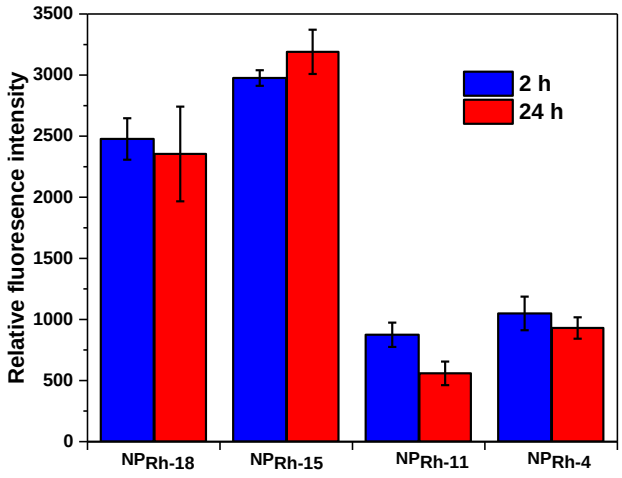

Fig. 8. Relative fluorescence intensity of **NP$_{Rh-n}$** (n = 4, 11, 15 and 18) in PC3 cells with a nanoparticle concentration of 100 μg mL^{-1} after 2 and 24 hours of incubation. Following background reduction using a roll ball model (25 μm), fluorescence associated with rhodamine (RFP filter, λ_{ex} = 531 nm, λ_{em} = 593 nm) was assigned as intracellular fluorescence. Data is represented as the arithmetic mean ± SD with experiments conducted in triplicate.

To further investigate cell uptake of **NP$_{Rh-n}$**, fluorescent confocal microscopy was used to track intracellular co-localisation. It was hypothesised that, due to their size, the nanoparticles would enter the cells through an energy dependent mechanism involving trafficking through a probable endosomal pathway.[50] It was therefore reasonable to assume possible trafficking of the nanoparticles to the lysosomes upon cellular entry. Thus, the PC3 cells were initially stained with lysosomal stain, lysotracker green, and incubated with **NP$_{Rh-18}$** (100 μg mL^{-1}). After 24 hours **NP$_{Rh-18}$** appears to be punctuated across the cell, with little co-localisation in the lysosomes (**Fig. 9**). This indicates that **NP$_{Rh-18}$** particles are either

able to escape along the endosomal pathway before reaching the lysosome or they enter the cell *via* an alternative mechanism.[51]

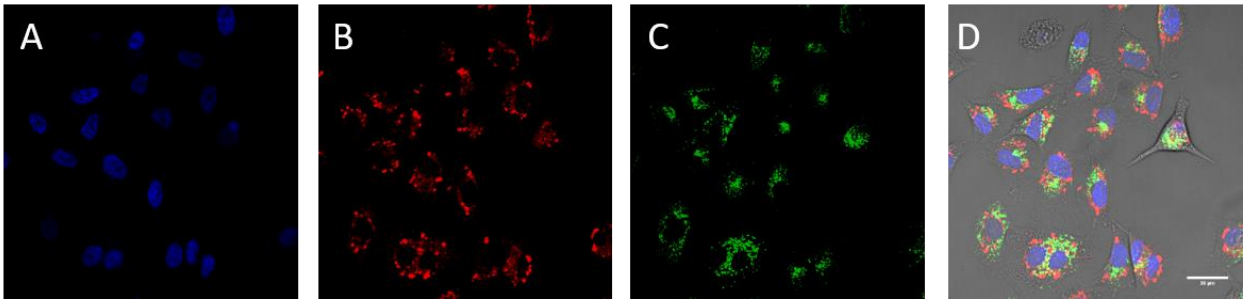

Fig. 9. Confocal fluorescent microscopy images of PC3 cells with $\mathbf{NP_{Rh\text{-}18}}$. (A) Hoechst 33258; (B) Rhodamine-B; (C) Lysotracker green; (D) Overlay of channels indicating lack of lysosomal co-localisation of the nanoparticles (scale bar = 30 μm)

Considering the biochemical affinity and activity of (in)organic arsenicals towards the mitochondria, mitochondrial co-localization of $\mathbf{NP_{Rh\text{-}18}}$ was then investigated. The mitochondria of PC3 cells were stained with mitotracker-green and incubated with $\mathbf{NP_{Rh\text{-}18}}$. Although the nanoparticles are distributed throughout the cell, there is juxtaposition of the mitochondrial and rhodamine stains indicative of co-localisation (**Fig. 10**). This can be attributed to targeting effects and the reactivity/affinity of unreacted AsAm groups present in the particles towards the mitochondria, as previously reported by Stenzel *et al*.[12, 13]

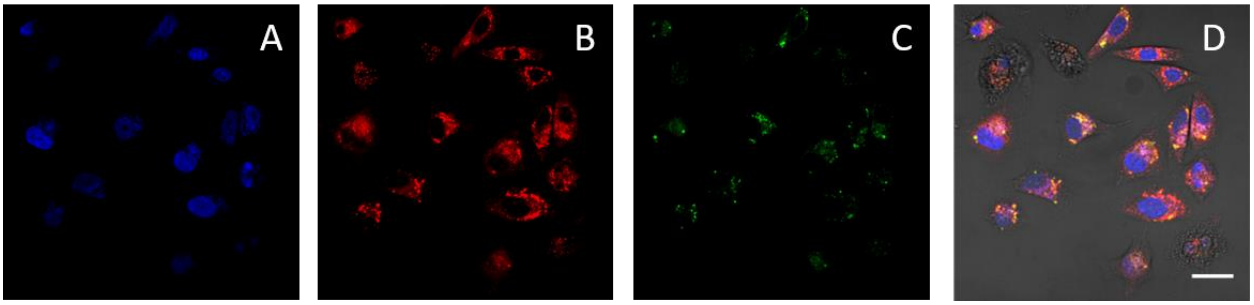

Fig. 10. Confocal fluorescent microscopy images of PC3 cells with $\mathbf{NP_{Rh\text{-}18}}$. (A) Hoechst 33258; (B) Rhodamine-B; (C) Mitotracker green; (D) Overlay of channels indicating lack of lysosomal co-localisation of the nanoparticles (scale bar = 30 μm)

Finally, to rule out that co-localisation of $\mathbf{NP_{Rh\text{-}18}}$ was as an artefact of diffusion of rhodamine leaching from the particles during the assay, co-localization assays were repeated using only free rhodamine. Although there appears to be some co-localization in the lysosome (**Fig. S23**), there is no evidence of co-localization in the mitochondria (**Fig. S24**) with rhodamine B appearing to be diffusely distributed throughout the cell.

The clinical success of arsenic trioxide (treatment of acute promyelocytic leukaemia) and organic arsenicals (for the treatment of much broader spectrum malignancies), relies on the synergy between chemical reactivity and biological activity of the arsenic functionality present. The apparent mitochondrial targeting properties of the polymeric arsenical nanoparticles reported here, along with the ability to tune stability, responsivity and functionality through the pendent AsAm groups (e.g. $\mathbf{NP_{As(I)}}$, $\mathbf{NP_{As\text{-}S}}$ and $\mathbf{NP_{V\text{-}As}}$) are attractive properties. In the long-term, the diverse chemistry of organic arsenicals and the potential for synergy between chemical and biological activity, could make polymeric arsenical nanomaterials viable candidates for drug-delivery and other chemotherapeutic applications.

CONCLUSION

Sequential reductive coupling and RCRAC, in the presence of functional acetylenes, has been introduced as a novel method to simultaneously assemble and cross-link thermoresponsive polymeric arsenical scaffolds (P(PEGA$_{20}$-*b*-[NIPAm$_{80\text{-}n}$-*co*-AsAm$_n$]); **P1**, n = 4; **P2**, n = 11; **P3**, n = 15; **P4**, n = 18). The resulting nanoparticles ($\mathbf{NP_{V\text{-}As}}$) are spherical with sizes < 35 nm and exhibit markedly enhanced stability under model biological redox conditions (GSH, H_2O_2, 5 mM) compared to related nanoparticles ($\mathbf{NP_{V\text{-}As}}$ > $\mathbf{NP_{As\text{-}S}}$ > $\mathbf{NP_{As(I)}}$). Propargyl alcohol, amine and propiolic acid were employed as functional acetylenes, demonstrating orthogonality of the RCRAC method with useful functional groups. Furthermore, use of propargyl-*O*-rhodamine B ester furnished fluorescent nanoparticles that were subsequently used to

investigate *in vitro* properties of **NP$_{V\text{-}As}$**. Polymers **P1** – **P4** and nanoparticles **NP$_{V\text{-}As}$** (**NP$_{PgOH\text{-}n}$**, **NP$_{PgNH\text{-}n}$**, **NP$_{PAc\text{-}n}$**, **NP$_{Rh\text{-}n}$**) all exhibited limited cytotoxicity *in vitro* against PC3 cells. Incubation of the fluorescent particles **NP$_{Rh\text{-}n}$** with PC3 cells, revealed cell uptake within 2 hours at 37 °C, while confocal microscopy using **NP$_{Rh\text{-}18}$** revealed co-localization in the mitochondria. This suggests that the **NP$_{Rh\text{-}18}$** either enter the cell *via* an expected endosomal pathway and then evade trafficking to the lysosome or alternatively, that they are internalized *via* a different uptake mechanism. Furthermore, the apparent affinity of **NP$_{Rh\text{-}18}$** for the mitochondria supports a working hypothesis, based on clinically relevant organic arsenicals and recently reported polymeric arsenical nanoparticles that exhibit high affinity and activity for the mitochondria, that polymeric arsenicals nanomaterials (**NP$_{V\text{-}As}$**, **NP$_{As\text{-}S}$**, **NP$_{As(I)}$**) could be viable candidates for drug delivery and other biomedical applications.

ASSOCIATED CONTENT

Supporting Information. Supplementary figures and tables corresponding the synthesis of **P1** – **P4** and fabrication of **NP$_{V\text{-}As}$** are presented in the supporting document which is available free of charge on the ACS Publications website.

AUTHOR INFORMATION

Corresponding Author

*Paul Wilson; p.wilson.1@warwick.ac.uk

Present Addresses

[ʃ] Department of Chemistry, University of North Carolina at Chapel Hill, Chapel Hill, North Carolina 27599-3290

[†] The Boots Science Building, School of Pharmacy, University Park, University of Nottingham, NG7 2RD

Author Contributions

The manuscript was written through contributions from all authors. All authors have given approval to the final version of the manuscript. ‡These authors contributed equally.

Funding Sources

Engineering and Physical Sciences Research Council (EPSRC); EP/F500378/1

Australian Research Council (ARC); CE140100036

Royal Society; URF\R1\180274

Leverhulme Trust; ECF/2015-075

ACKNOWLEDGMENT

The authors gratefully acknowledge financial support from Engineering and Physical Sciences Research Council (EPSRC) under grant EP/F500378/1 through the Molecular Organization and Assembly in Cells Doctoral Training Centre (MOAC-DTC). The authors also wish to acknowledge the facilities and personnel enabled by the Monash-Warwick Alliance. This work was carried out in conjunction with the Australian Research Council (ARC) Centre of Excellence in Convergent Bio-NanoScience and Technology (CE140100036). P.W. thanks the Leverhulme Trust for the award of an Early Career Fellowship (ECF/2015-075) and the Royal Society and Tata companies for the award of a University Research Fellowship (URF\R1\180274). The authors would like to thank the Polymer Characterization and Microscopy Research Technology Platform for access and use of SEC, AFM and TEM facilities.

REFERENCES

1. Z.-Y. Wang and Z. Chen, *Blood*, 2008, **111**, 2505-2515.
2. L. Horsley, J. Cummings, M. Middleton, T. Ward, A. Backen, A. Clamp, M. Dawson, H. Farmer, N. Fisher, G. Halbert, S. Halford, A. Harris, J. Hasan, P. Hogg, G. Kumaran, R. Little, G. J. M. Parker, P. Potter, M. Saunders, C. Roberts, D. Shaw, N. Smith, J. Smythe, A. Taylor, H. Turner, Y. Watson, C. Dive and G. C. Jayson, *Cancer Chemother. Pharmacol.*, 2013, **72**, 1343-1352.

3. P. J. Dilda, S. Decollogne, L. Weerakoon, M. D. Norris, M. Haber, J. D. Allen and P. J. Hogg, *J. Med. Chem.*, 2009, **52**, 6209-6216.
4. J. Wu, F. Muggia, C. Henderson, L. Feun, P. V. Veldhuizen, P. Gold, H. Zheng, G. A. 66201, J. Lewis and A. X. Zhu, *J. Clin. Oncol.*, 2009, **27**, e15630-e15630.
5. A. M. Spuches, H. G. Kruszyna, A. M. Rich and D. E. Wilcox, *Inorg. Chem.*, 2005, **44**, 2964-2972.
6. V. P. Whittaker, *Biochem. J.*, 1947, **41**, 56-62.
7. S. Shen, X.-F. Li, W. R. Cullen, M. Weinfeld and X. C. Le, *Chem. Rev.*, 2013, **113**, 7769-7792.
8. D. Fass and C. Thorpe, *Chemical Reviews*, 2018, **118**, 1169-1198.
9. D. Ramadan, P. C. Rancy, R. P. Nagarkar, J. P. Schneider and C. Thorpe, *Biochemistry*, 2009, **48**, 424-432.
10. D. Park, J. Chiu, G. G. Perrone, P. J. Dilda and P. J. Hogg, *Cancer Cell Int.*, 2012, **12**, 11.
11. J. Tanaka, T. P. Davis and P. Wilson, *Macromol. Rapid Commun.*, 2018, **39**, 1800205.
12. J.-M. Noy, H. Lu, P. J. Hogg, J.-L. Yang and M. Stenzel, *Bioconjugate Chem.*, 2018, **29**, 546-558.
13. J.-M. Noy, C. Cao and M. Stenzel, *ACS Macro Lett.*, 2019, **8**, 57-63.
14. P. Wilson, A. Anastasaki, M. R. Owen, K. Kempe, D. M. Haddleton, S. K. Mann, A. P. R. Johnston, J. F. Quinn, M. R. Whittaker, P. J. Hogg and T. P. Davis, *J. Am. Chem. Soc.*, 2015, **137**, 4215-4222.
15. C. Footman, P. A. J. M. de Jongh, J. Tanaka, R. Peltier, K. Kempe, T. P. Davis and P. Wilson, *Chem. Commun.*, 2017, **53**, 8447-8450.
16. J. Tanaka, S. Tani, R. Peltier, E. H. Pilkington, A. Kerr, T. P. Davis and P. Wilson, *Polym. Chem.*, 2018, **9**, 1551-1556.
17. J. Tanaka, J.-I. Song, A. M. Lunn, R. A. Hand, S. Häkkinen, T. L. Schiller, S. Perrier, T. P. Davis and P. Wilson, *J. Mater. Chem. B*, 2019, **7**, 4263-4271.
18. J. Tanaka, G. Moriceau, A. Cook, A. Kerr, J. Zhang, R. Peltier, S. Perrier, T. P. Davis and P. Wilson, *Macromolecules*, 2019, **52**, 992-1003.
19. L. R. Smith and J. L. Mills, *J. Organomet. Chem.*, 1975, **84**, 1-15.
20. H. J. Breunig, in *Organic Arsenic, Antimony and Bismuth Compounds (1994)*, John Wiley & Sons, Ltd, 2004, DOI: 10.1002/0470023473.ch14, pp. 563-577.
21. J. W. B. Reesor and G. F. Wright, *J. Org. Chem.*, 1957, **22**, 382-385.
22. N. C. Lloyd, H. W. Morgan, B. K. Nicholson and R. S. Ronimus, *Angew. Chem. Int. Ed.*, 2005, **44**, 941-944.
23. K. Naka, T. Umeyama and Y. Chujo, *J. Am. Chem. Soc.*, 2002, **124**, 6600-6603.
24. C. J. Ferguson, R. J. Hughes, D. Nguyen, B. T. T. Pham, R. G. Gilbert, A. K. Serelis, C. H. Such and B. S. Hawkett, *Macromolecules*, 2005, **38**, 2191-2204.
25. A. Schachtschneider, M. Wessig, M. Spitzbarth, A. Donner, C. Fischer, M. Drescher and S. Polarz, *Angew. Chem. Int. Ed.*, 2015, **54**, 10465-10469.
26. K. Naka, A. Nakahashi, M. Bravo and Y. Chujo, *Appl. Organomet. Chem.*, 2010, **24**, 573-575.
27. K. Naka and Y. Chujo, in *Conjugated Polymer Synthesis*, Wiley-VCH Verlag GmbH & Co. KGaA, 2010, DOI: 10.1002/9783527632664.ch9, pp. 229-249.
28. T. Umeyama, K. Naka and Y. Chujo, *J. Polym. Sci. Part A: Polym. Chem.*, 2004, **42**, 3604-3611.
29. K. Naka, A. Nakahashi and Y. Chujo, *Macromolecules*, 2006, **39**, 8257-8262.
30. K. Naka, A. Nakahashi and Y. Chujo, *Macromolecules*, 2007, **40**, 1372-1376.
31. T. Umeyama, K. Naka and Y. Chujo, *Macromolecules*, 2004, **37**, 5952-5958.
32. T. Umeyama, K. Naka, A. Nakahashi and Y. Chujo, *Macromolecules*, 2004, **37**, 1271-1275.
33. T. Umeyama, K. Naka and Y. Chujo, *J. Polym. Sci. Part A: Polym. Chem.*, 2004, **42**, 3023-3028.

34. T. Umeyama, K. Naka and Y. Chujo, *Macromolecules*, 2004, **37**, 3623-3629.
35. D. B. Sowerby, in *Organic Arsenic, Antimony and Bismuth Compounds (1994)*, DOI: 10.1002/0470023473.ch2, pp. 25-88.
36. X. Guo, Y. Cheng, X. Zhao, Y. Luo, J. Chen and W.-E. Yuan, *J. Nanobiotechnol.*, 2018, **16**, 74-74.
37. S. Kwon, H. Ko, D. G. You, K. Kataoka and J. H. Park, *Acc. Chem. Res.*, 2019, **52**, 1771-1782.
38. F. Meng, W. E. Hennink and Z. Zhong, *Biomaterials*, 2009, **30**, 2180-2198.
39. C. de Gracia Lux, S. Joshi-Barr, T. Nguyen, E. Mahmoud, E. Schopf, N. Fomina and A. Almutairi, *J. Am. Chem. Soc.*, 2012, **134**, 15758-15764.
40. F. Alexis, E. Pridgen, L. K. Molnar and O. C. Farokhzad, *Mol. Pharm.*, 2008, **5**, 505-515.
41. N. P. Truong, M. R. Whittaker, C. W. Mak and T. P. Davis, *Expert Opin. Drug Delivery*, 2015, **12**, 129-142.
42. K. S. Ho and M. S. Shoichet, *Curr. Opin. Chem. Eng.*, 2013, **2**, 53-59.
43. J. C. Zhao, H. X. Lu, S. Wong, M. X. Lu, P. Xiao and M. H. Stenzel, *Polym. Chem.*, 2017, **8**, 3317-3326.
44. Y. Kim, M. H. Pourgholami, D. L. Morris and M. H. Stenzel, *Biomacromolecules*, 2012, **13**, 814-825.
45. S. Kaga, N. P. Truong, L. Esser, D. Senyschyn, A. Sanyal, R. Sanyal, J. F. Quinn, T. P. Davis, L. M. Kaminskas and M. R. Whittaker, *Biomacromolecules*, 2017, **18**, 3963-3970.
46. H. Cabral, Y. Matsumoto, K. Mizuno, Q. Chen, M. Murakami, M. Kimura, Y. Terada, M. R. Kano, K. Miyazono, M. Uesaka, N. Nishiyama and K. Kataoka, *Nat. Nanotechnol.*, 2011, **6**, 815.
47. M. E. Davis, Z. Chen and D. M. Shin, in *Nanoscience and Technology*, DOI: 10.1142/9789814287005_0025, pp. 239-250.
48. A. G. Torres and M. J. Gait, *Trends in Biotechnol.*, 2012, **30**, 185-190.
49. N. Donoghue, P. T. Yam, X. M. Jiang and P. J. Hogg, *Protein Sci.*, 2000, **9**, 2436-2445.
50. G. J. Doherty and H. T. McMahon, *Annu. Rev. Biochem.*, 2009, **78**, 857-902.
51. L. Shang, K. Nienhaus and G. U. Nienhaus, *J. Nanobiotechnol.*, 2014, **12**, 5.

TOC ENTRY

Functional and stable polymeric arsenical nanoparticles can be prepared by sequential reductive coupling and ring-collapse radical alternating copolymerisation (RCRAC).

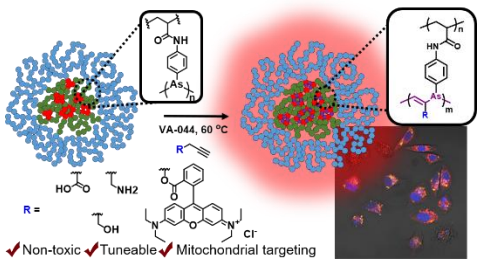
VA-044, 60 °C
R =
Non-toxic
Tuneable
Mitochondrial targeting